

Numerical simulation of transient development and diminution of weld pool in gas tungsten arc welding

Chuan Song Wu and Fengjie Yan

MOE Key Lab of LMSH, Institute for Materials Joining, Shandong University,
Peoples' Republic of China

Received 3 April 2003, in final form 31 July 2003

Published 3 November 2003

Online at stacks.iop.org/MSMSE/12/13 (DOI: 10.1088/0965-0393/12/1/002)

Abstract

A mathematical model has been developed to describe the transient heat and fluid flow fields in gas tungsten arc welding (GTAW). The transient development and diminution of the weld pool at two periods after the arc ignites and extinguishes are analysed quantitatively. The data for the weld pool configurations under different welding conditions from the transient state to the quasi-steady state are obtained. The time for the weld pool shape to reach the quasi-steady state and the time for the weld pool to solidify completely are predicted. GTAW experiments show that the predictions of the weld pool shape based on the model are in agreement with the measured values. The numerical results of the dynamic development and diminution of weld pool configurations could be used to correlate the transient characteristics of weld pool behaviour with the occurrence of weld formation defects.

1. Introduction

It is well known that the dynamic behaviour of weld pools, due to heat and fluid flow in the weld pool, has significant influence on the temperature distribution, shape and size of the weld pool, final solidification microstructures, and consequently the resultant mechanical properties of the welded joints [1]. It is of great significance to understand the dynamics of the weld pool quantitatively. There have been significant advances in the numerical simulations of weld pool behaviour [2–7]. However, most investigations have focused on modelling weld pool behaviour in a quasi-steady state, and little attention has been paid to the transient dynamics of the weld pool, especially the transient heating period after the arc ignites and the transient cooling period after the arc extinguishes. In fact, when the arc ignites during the initiation of welding, the weld pool develops and expands gradually, whereas the weld pool reduces quickly after the arc extinguishes when welding ends. The transient state of the weld pool may result in some weld defects such as humped beads and undercutting [8]. Thus, the transient heat and fluid flow phenomena of the weld pool should be addressed adequately. This paper introduces such a model.

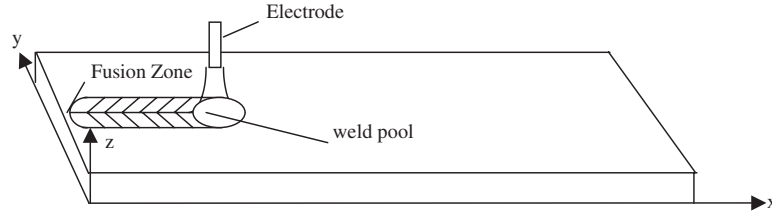


Figure 1. Sketch of the TIG welding system.

2. Formulation

Figure 1 shows the schematic sketch of the gas tungsten arc welding (GTAW) system. After the arc ignites, the workpiece is heated and melted so that the weld pool emerges. The volume of the weld pool expands until a quasi-steady state is reached. Then, the weld pool travels along the welding direction with the same speed as the arc. When the arc extinguishes, the weld pool stops travelling and reduces rapidly. In order to model the dynamic development of the weld pool for the whole welding process, the transient state of the temperature and the fluid flow fields must be considered. Besides, the following assumptions have been adopted: (1) the flow is Newtonian, incompressible and laminar, (2) latent heat is not considered, (3) the mushy zone between liquids and solids is not considered and (4) the surface of the weld pool is flat. Assumption 2 is reasonable because exclusion of latent heat may cause only a small difference in the computed weld pool shape, but would simplify the computational procedure [9–12]. The assumption of a flat pool surface is based on the fact that the surface deformation of the weld pool is very small in GTAW when the current is below 220 A [13]. The governing equations for describing the dynamic fluid flow and heat transfer in the weld pool are as follows:

$$\frac{\partial u}{\partial x} + \frac{\partial v}{\partial y} + \frac{\partial w}{\partial z} = 0 \quad (1)$$

$$\rho C_p \left(\frac{\partial T}{\partial t} + u \frac{\partial T}{\partial x} + v \frac{\partial T}{\partial y} + w \frac{\partial T}{\partial z} \right) = \frac{\partial}{\partial x} \left(k \frac{\partial T}{\partial x} \right) + \frac{\partial}{\partial y} \left(k \frac{\partial T}{\partial y} \right) + \frac{\partial}{\partial z} \left(k \frac{\partial T}{\partial z} \right) \quad (2)$$

$$\rho \left(\frac{\partial u}{\partial t} + u \frac{\partial u}{\partial x} + v \frac{\partial u}{\partial y} + w \frac{\partial u}{\partial z} \right) = -\frac{\partial P}{\partial x} + \mu \left(\frac{\partial^2 u}{\partial x^2} + \frac{\partial^2 u}{\partial y^2} + \frac{\partial^2 u}{\partial z^2} \right) + F_x \quad (3)$$

$$\rho \left(\frac{\partial v}{\partial t} + u \frac{\partial v}{\partial x} + v \frac{\partial v}{\partial y} + w \frac{\partial v}{\partial z} \right) = -\frac{\partial P}{\partial y} + \mu \left(\frac{\partial^2 v}{\partial x^2} + \frac{\partial^2 v}{\partial y^2} + \frac{\partial^2 v}{\partial z^2} \right) + F_y \quad (4)$$

$$\rho \left(\frac{\partial w}{\partial t} + u \frac{\partial w}{\partial x} + v \frac{\partial w}{\partial y} + w \frac{\partial w}{\partial z} \right) = -\frac{\partial P}{\partial z} + \mu \left(\frac{\partial^2 w}{\partial x^2} + \frac{\partial^2 w}{\partial y^2} + \frac{\partial^2 w}{\partial z^2} \right) + F_z \quad (5)$$

where u , v , w are the velocity components in the x -, y - and z -directions, respectively, T is the temperature, ρ is the density, C_p is the specific heat, k is the thermal conductivity, μ is the viscosity, P is the pressure, F_x , F_y and F_z are the components of the body force term in the x -, y - and z -directions, respectively.

For describing the heat source, a modified Gaussian distribution model of the arc heat flux is employed. It uses two double ellipsoids in the following form [14]:

$$q_f(x, y) = \frac{6Q_f}{\pi a c_1} \exp\left(-\frac{3x^2}{c_1^2}\right) \exp\left(-\frac{3y^2}{a^2}\right) \quad x \geq 0 \quad (6)$$

$$q_f(x, y) = \frac{6Q_r}{\pi a c_2} \exp\left(-\frac{3x^2}{c_2^2}\right) \exp\left(-\frac{3y^2}{a^2}\right) \quad x < 0 \quad (7)$$

where $Q_f = (c_1 \eta IU)/(c_1 + c_2)$, $Q_r = (c_2 \eta IU)/(c_1 + c_2)$, $q_f(x, y)$ is the heat flux, c_1 and c_2 are dependent on the welding process parameters, I is the welding current, U is the arc voltage and η is the arc power efficiency.

On the workpiece surface, there is loss of heat due to convection and radiation,

$$q_{\text{conv}} = h_c(T - T_0) \quad (8)$$

where h_c is the heat transfer coefficient due to convection and radiation, and T_0 is the ambient temperature. h_c is temperature dependent [14]:

$$h_c = 24.1 \times 10^{-4} \times \varepsilon \times T^{1.61} \quad (9)$$

where ε is the emissivity.

The heat flux evaporated from the central region of the weld pool can be estimated by the following equations [15]:

$$q_{\text{evp}} = W_v h_{\text{fg}} \quad (10)$$

where h_{fg} is the latent heat of evaporation, W_v is the evaporation rate,

$$\log W_v = A_v + \log P_{\text{atm}} - 0.5 \log T \quad (11)$$

where P_{atm} is the pressure at which evaporation occurs, A_v is a constant.

The boundary conditions for equation (2) are as follows:

At the upper surface of the workpiece,

$$k \frac{\partial T}{\partial z} = q_{\text{arc}} - q_{\text{conv}} - q_{\text{evap}}. \quad (12)$$

At the lower surface of the workpiece,

$$k \frac{\partial T}{\partial z} = -q_{\text{conv}}. \quad (13)$$

At other surfaces of the workpiece,

$$k \frac{\partial T}{\partial r} = -q_{\text{conv}}. \quad (14)$$

The boundary conditions for equations (3)–(5) take the following form:

At the upper surface of the weld pool,

$$\mu \frac{\partial u}{\partial z} = -\frac{\partial \gamma}{\partial T} \frac{\partial T}{\partial x} \quad (15)$$

$$\mu \frac{\partial v}{\partial z} = -\frac{\partial \gamma}{\partial T} \frac{\partial T}{\partial y} \quad (16)$$

$$w = 0 \quad (17)$$

where γ is the surface tension.

In the solid region,

$$u = 0, \quad v = 0, \quad w = 0. \quad (18)$$

At the lower surface of the weld pool if full penetration is reached:

$$\mu \frac{\partial u}{\partial z} = -\frac{\partial \gamma}{\partial T} \frac{\partial T}{\partial x} \quad (19)$$

$$\mu \frac{\partial v}{\partial z} = -\frac{\partial \gamma}{\partial T} \frac{\partial T}{\partial y} \quad (20)$$

$$w = 0. \quad (21)$$

For the body force term in the momentum equation, the same method is employed as introduced in [11].

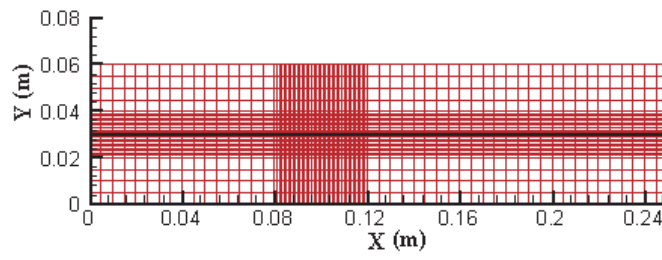


Figure 2. Non-uniform mesh.

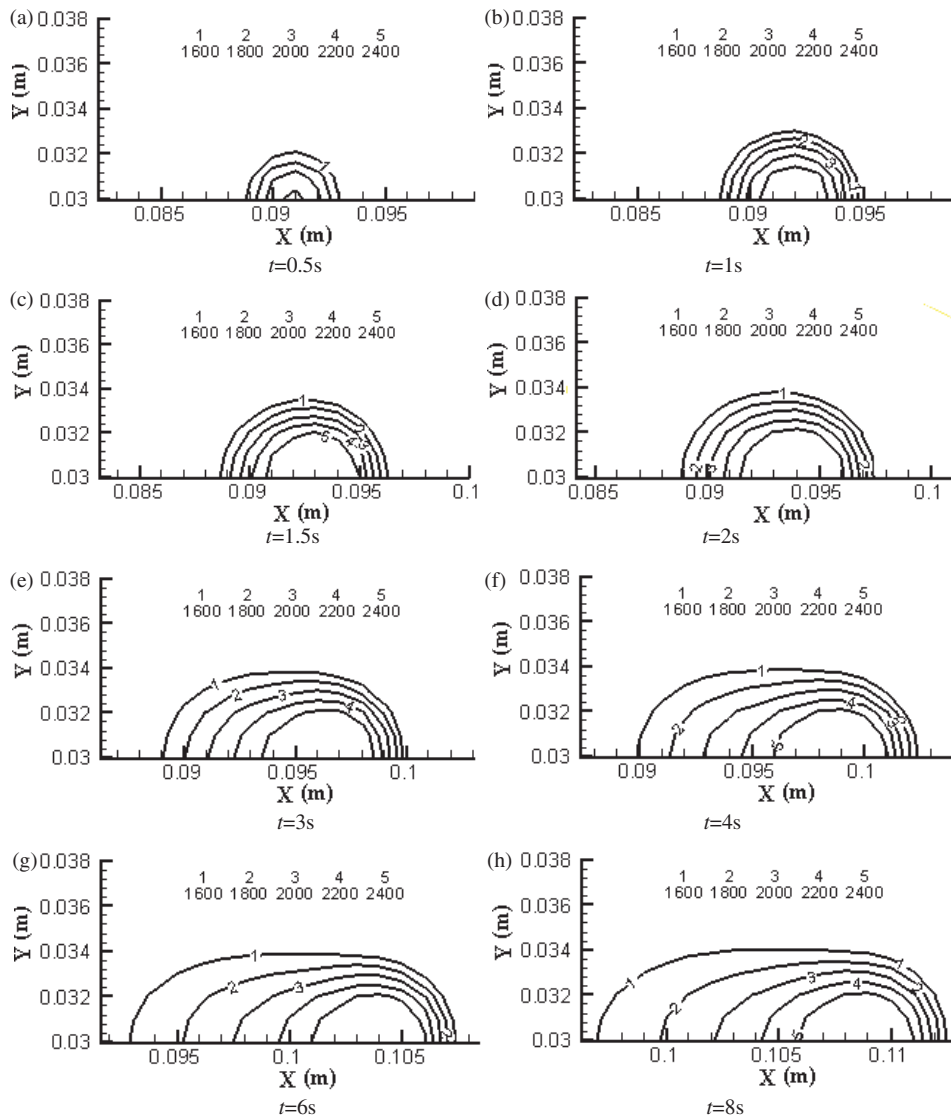


Figure 3. The calculated temperature distribution on the upper surface of the workpiece at different times, after igniting the arc (workpiece: mild steel, $v_0 = 2.5 \text{ mm s}^{-1}$, $U = 16 \text{ V}$, $I = 100 \text{ A}$).

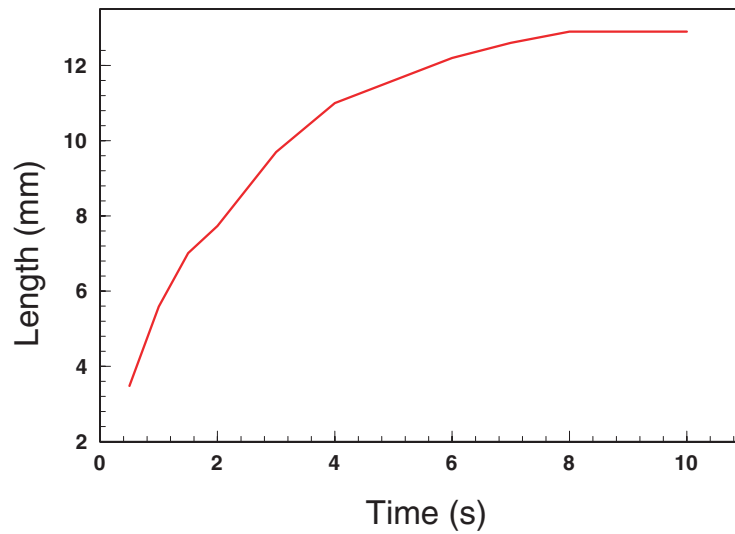


Figure 4. The relation between the length of the weld pool and the welding time after igniting the arc (workpiece: mild steel, $v_0=2.5 \text{ mm s}^{-1}$, $U = 16 \text{ V}$, $I = 100 \text{ A}$).

3. Results and discussion

It is very important to select the proper grid size and time step in the numerical simulation of fluid flow and heat transfer in weld pools. The criteria are whether the calculation precision is satisfactory and the length of calculating time is acceptable. The grid system shown in figure 2 is used in the calculation. The finer grids are put around the heat source. Finer time steps are employed at the initial phase of the calculation. The workpiece is of dimensions $250 \text{ mm} \times 60 \text{ mm} \times 2 \text{ mm}$. The weld centreline is at a y -coordinate of 0.03 m , as shown in figure 2. The arc moves along the x -direction with a starting point of the x -coordinate at 0.09 m . The values of the thermal property parameters used in the calculation are given in [12].

Figure 3 shows the predicted temperature distribution at the upper surface of the workpiece. It can be seen that the isothermal enclosures expand as time progresses after the arc ignites. The isothermal enclosures are moving with the arc along the x -direction. Figures 4 and 5 show the relation between the weld pool length and width and the welding time. As the welding time increases, both the pool length and width increase, but the pool width grows more quickly. When the welding is conducted for about 5 s , the pool width reaches its quasi-steady state condition, whereas it takes about 12 s for the pool length to reach the quasi-steady state condition. Figure 6 shows the weld pool shape at the workpiece surface after the arc extinguishes. Because there is no further heat input, the weld pool contracts quickly as time increases. At about 0.7 s after the arc has extinguished, the weld pool solidifies completely. Figure 7 illustrates the fluid flow field at the surface of the weld pool.

GTAW experiments are conducted to measure the weld pool geometry to verify the calculated results. A specially designed visual sensor is used to capture the weld pool images during the GTAW process [16]. Figure 8 makes a comparison of the predicted weld pool surface geometry with the measured one under different welding process parameters. It can be seen that both match to a reasonable precision.

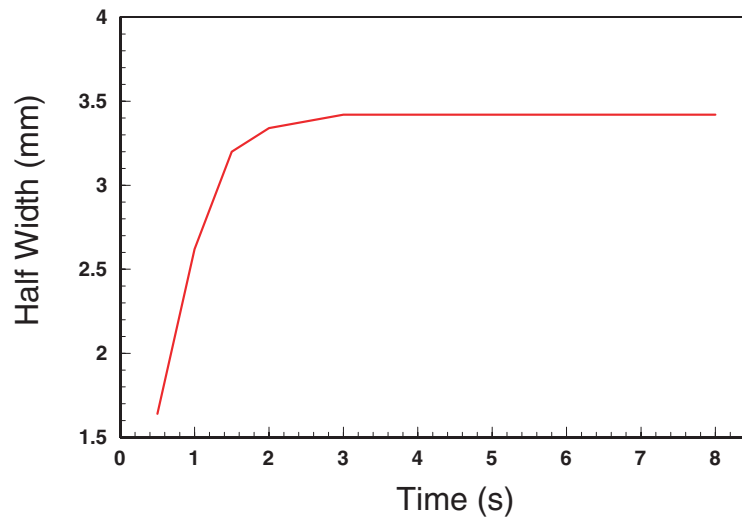


Figure 5. The relation between the half-width of the weld pool and the welding time after igniting the arc (workpiece: mild steel, $v_0 = 2.5 \text{ mm s}^{-1}$, $U = 16 \text{ V}$, $I = 100 \text{ A}$).

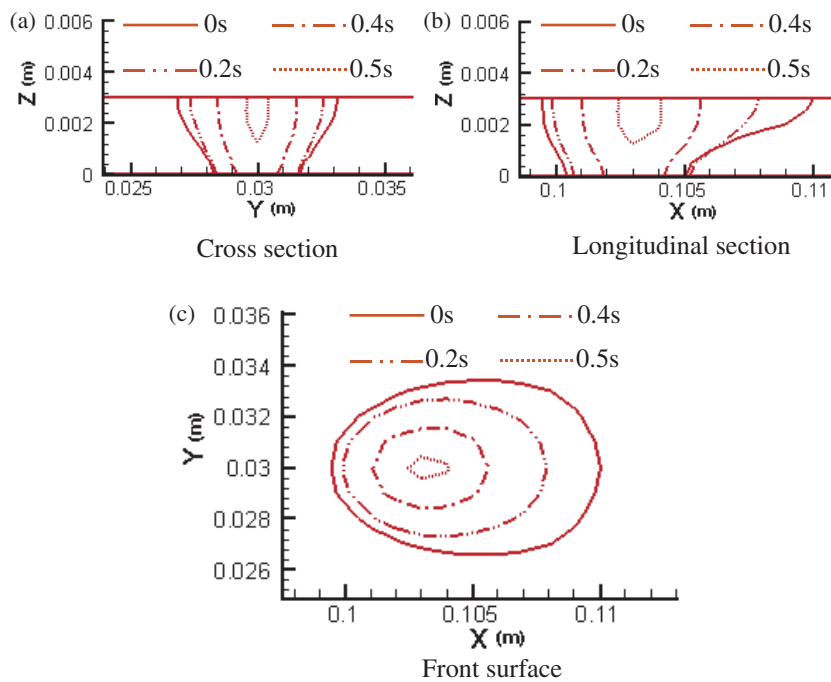


Figure 6. The calculated surface geometry of the weld pool after the arc is extinguished (workpiece: mild steel, $v_0 = 1.517 \text{ mm s}^{-1}$, $U = 16 \text{ V}$, $I = 100 \text{ A}$).

4. Conclusion

A mathematical model has been developed to describe the transient heat and fluid flow fields in GTAW. The dynamic development of the weld pool geometry after the arc ignites is analysed

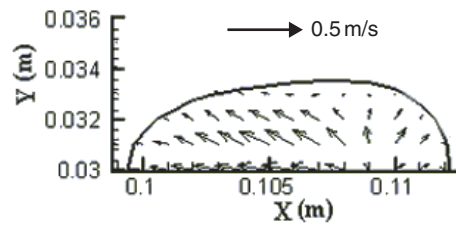


Figure 7. Calculated results of the fluid flow field in the GTAW weld pools (on the upper surface) (workpiece: mild steel, $v_0 = 1.517 \text{ mm s}^{-1}$, $U = 16 \text{ V}$, $t = 12 \text{ s}$).

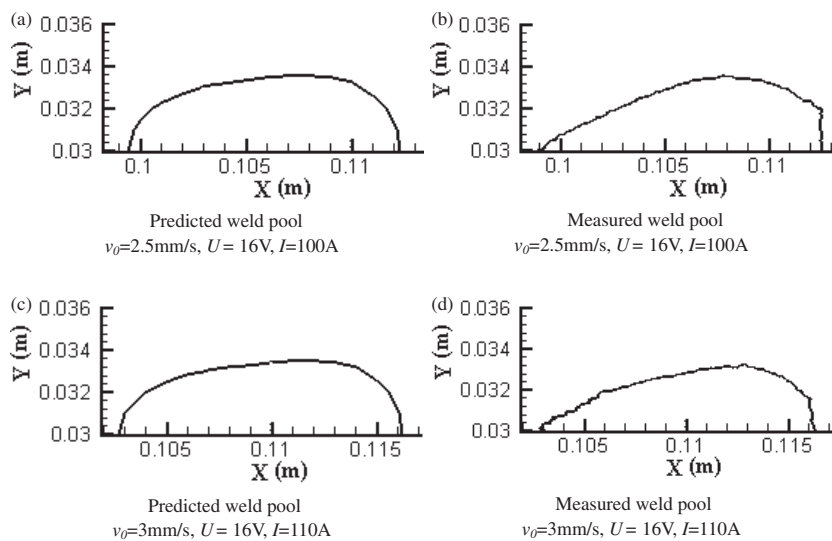


Figure 8. The predicted and measured weld pools (on the upper surface) under different welding parameters (workpiece: mild steel).

quantitatively. The time for the weld pool shape to reach the quasi-steady state is determined. The diminishing process of the weld pool after the arc extinguishes is simulated, and the time for the whole weld pool to solidify completely is predicted. The measured surface shape of the weld pool, using a visual system, during the GTAW process is in agreement with the calculated values. This work could lay the foundation for the numerical analysis of the relation between the transient characteristics of weld pool behaviour and the occurrence of weld formation defects.

References

- [1] David S A, Vitek J M, Zacharia T and DebRoy T 1993 Weld pool phenomena *Int. Inst. Weld. Doc.* **212-829-93** 2-4
- [2] Choo R T C 1990 Modeling of high-current arcs with emphasis on free surface phenomena in the weld pool *Weld. J.* **69** 346s-61s
- [3] Li Z Y and Wu C S 1997 Analysis of the transport phenomena in the interfacial region between TIG arcs and weld pools *Comput. Mater. Sci.* **8** 243-50

- [4] Kou S 1986 Weld pool convection and its effect *Weld. J.* **65** 63s–70s
- [5] Ko S H, Choi S K and Yoo C D 2001 Effect of surface depression on pool convection and geometry in stationary GTAW *Weld. J.* **80** 39s–45s
- [6] Wang Y, Shi Q and Tsai H L 2001 Modeling of the effects of surface-active elements on flow patterns and weld penetration *Metall. Mater. Trans. B* **32** 145–61
- [7] Wu C S and Zheng W 1997 Analysis of fluid flow and heat transfer in a moving pulsed TIG weldpool *Int. J. Joining Mater.* **8** 243–50
- [8] Feng L, Chen S and Yin S 1999 The formation mechanism of weld undercut in high-speed welding *Trans. China Weld. Inst.* **20** 16–21
- [9] Zacharia T, David S A, Vitek J M and DebRoy T 1989 Heat transfer during Nd: Yag pulsed laser welding and its effect on solidification structure of austenitic stainless steels *Metall. Trans. A* **20** 957–67
- [10] Oreper G M, Eagar T W and Szekely J 1983 Convection in arc weld pool *Weld. J.* **62** 307s–12s
- [11] Wu C S and Dorn L 1994 Computer simulation of fluid dynamics and heat transfer in full-penetrated TIG weld pools with surface depression *Comput. Mater. Sci.* **2** 341–9
- [12] Wu C S and Tsao K C 1990 Modeling the three-dimensional fluid flow and heat transfer in a moving weld pool *Eng. Comput.* **7** 241–8
- [13] Lin M L and Eagar T W 1985 Influence of arc pressure on weld pool geometry *Weld. J.* **64** 163s–9s
- [14] Goldak J, Chakravarti A and Bibby M 1984 A new finite element model for welding heat sources *Metall. Trans. B* **15** 299–305
- [15] Choi M and Greif R 1987 A study of the heat transfer during arc welding with applications to pure metals or alloys and low or high boiling temperature materials *Numer. Heat Transfer* **11** 477–89
- [16] Gao J Q and Wu C S 2001 Experimental determination of weld pool geometry in gas tungsten arc welding *Sci. Technol. Weld. Joining* **6** 288–92